Promotional Effect of Zirconium Doping on the NH_3-SCR Activity of CeO_2 and CeO_2-TA Modified by Thiourea: A Comparative Study

Jun Li[1], Fei Zhou[1,2], Zhibo Xiong[1*], Yanping Du[3], Qiguo Yang[1], Wei Wang[1], Wei Lu[1]

1. School of Energy and Power Engineering, University of Shanghai for Science & Technology, Shanghai, 200093, China

2. Jiangsu Guoxin Jingjiang Power Co. Ltd., Jingjiang 214500, Jiangsu, China

3. Department of Engineering, Faculty of Environment, Science and Economy, University of Exeter, Penryn Campus, Penryn, Cornwall TR109FE, UK

CRediT authorship contribution statement

Jun Li: Methodology, Writing - original draft. **Fei Zhou:** Investigation, Supervision. **Zhibo Xiong:** Conceptualization, Funding acquisition, Writing-review & editing. Yanping Du: Writing-review & editing**. Qiguo Yang:** Investigation, Supervision. **Wei Wang:** Investigation, Supervision. **Wei Lu:** Investigation, Supervision, Funding acquisition.

Abstract:

Herein, zirconium(Zr) was doped to optimize the NH_3-SCR activity of both CeO_2 and thiourea modified CeO_2-TA catalysts for comparison. Different from the promotional influence of thiourea modification on the agglomeration of CeO_2, the transformation from nanoparticles to nanocubes and the formation of highly crystallized $CeOSO_4$, Zr doping lowers the agglomeration of nanoparticles, loosens the surface morphology of catalyst and promotes the formation of Ce-Zr solid solution. Furthermore, Zr doping exhibits a synergistic promotional effect of thiourea modification on the dispersion of Ce^{3+} and S^{6+} species on the surface of CeO_2, and increases the concentrations of the surface total oxygen and chemisorbed oxygen of CeO_2-TA. Interestingly, Zr doping instead decreases the promotional effect of thiourea modification on the high-temperature or medium/low-

temperature reducibility of catalyst, but increases both Brønsted and lewis acid sites of CeO_2-TA by inducing the highly dispersive sulfate species rather than the $CeOSO_4$ crystal, which might be crucial to the NH_3-SCR activity of Ce-based catalyst.

Introduction

The emission of nitrogen oxides (NO_x) from stationary and mobile sources is harmful to human health and global environment. Selective catalytic reduction with ammonia (NH_3-SCR) has been widely used to reduce NO_x because of the attractive removal efficiency, stability and selectivity.[1] Meanwhile, there still remains some problems needing to be concerned and overcome for the commercial V_2O_5-WO_3/TiO_2 catalyst, for example, the toxicity of vanadium, the narrow working temperature window, the low N_2 selectivity and the high conversion of SO_2 to SO_3 with increasing vanadium loadings.[2] Therefore, it is very necessary to develop a novel non-vanadium-based catalyst with excellent NH_3-SCR activity and N_2 selectivity in a wide temperature range. Owing to the efficient electronic migration between Ce^{4+} and Ce^{3+}, cerium dioxide (CeO_2) presents an outstanding oxygen storage capacity and remarkable reducibility with rich oxygen defects, thus Ce-based catalyst has attracted widespread attention in the fields of heterogeneous catalysis, including photocatalysis,[3] catalytic reforming,[4] catalytic oxidation,[5] NH_3-SCR,[6] and so on.[7]

Nevertheless, pure CeO_2 exhibits poor catalytic performance of NO_x reduction and N_2 selectivity due to the lack of surface acidity, the small specific surface area and the limited redox property. Therefore, some metal and non-metallic ions have been introduced to optimize the NH_3-SCR activity of ceria. For instance, WO_3,[8] MoO_3,[9] ZrO_2,[10] and Nb_2O_5[11] have been used to improve the NH_3-SCR activity of Ce-based catalyst via enhancing its surface acidity. In addition, the transition metal elements with variable valences have been confirmed to optimize the redox

properties of Ce-based catalyst by inducing a new redox cycle on the basis of Ce^{4+}/Ce^{3+} ion pair,[12] for example, $Ce^{4+} + Fe^{2+} \leftrightarrow Ce^{3+} + Fe^{3+}$ for Fe doping.[13] Among the metal ion additives investigated, zirconium presents a good promotional effect on the NH_3-SCR activity of cerium-based catalyst owing to the increased surface acidity and the formed Ce-Zr solid solution.[14] Furthermore, the selecting of Ce/Zr molar ratio could regulate the lattice parameters and physicochemical properties of Ce-Zr solid solution, thus affects the dispersion of other active components on catalyst surface and the NH_3-SCR activity.[15] Zhao et al.[16] had investigated the influence of Zr doping molar ratio on the oxygen storage capacity (OSC) and thermal stability of Ce-Zr solid solution synthesized via the flame spray pyrolysis, and found that the appropriate molar ratio of Zr doping helped to improve the formation of oxygen vacancies and the mobility of active oxygen on the surface of Ce-Zr solid solution. Prasad et al.[17] pointed out that the formation of Ce-Zr solid solution after Zr doping increased the oxygen mobility, OSC and reducibility of the synthesized Ni/$Ce_xZr_{1-x}O_2$ catalyst accompanied by the optimization of Ni dispersion, and the studies of density functional theory (DFT) demonstrated that $Ce_{0.5}Zr_{0.5}O_z$ exhibited the lowest oxygen vacancy formation energy (OVFE), thus presented the strongest oxygen storage capacity. Interestingly, the doping of Zr has also been found to optimize the structural and physicochemical properties of ceria which are crucial to the NH_3-SCR activity of catalyst. Yao et al.[18] had found that the doping of Zr with its molar ratio of Zr/(Ce+Zr) being 0.1 helped to promote the dispersion of active substances due to the increased BET surface area, and simultaneously adjusted the redox properties and enhanced the surface acidity of the as-prepared catalyst. It is noteworthy that when the molar ratio of Zr/(Ce+Zr) is less than 0.06, Zr ions tend to substitute the Ce sites and results in the lattice distortion of ceria, but the excess Zr ions can occupy the interstitial sites or/and surface

of ceria when the Zr/(Ce+Zr) molar ratio exceeds 0.06.[19] It had been reported that the enhancement of Zr doping molar ratio (Zr/(Ce+Zr)) to 10% obviously increased the redox ability of cerium oxide, but the further increase of Zr doping amount only changed the reducibility of catalyst and the suitable Zr molar ratio was about 10%.[20] Therefore, the doping of low-quality Zr could also enrich the oxygen vacancies of CeO_2 and improve its redox ability.

In order to optimize the surface acidity and redox properties of cerium-based catalyst, some non-metal ions, including N, P and S, have also been introduced in different forms via various preparation methods.[21] Cong et al.[22] had verified that the doping of N not only enriched the Brönsted acid sites of CeO_2, but also facilitated the generation of active nitrite species, thus improved its high temperature NH_3-SCR activity by inhibiting the catalytic oxidation of the adsorbed NH_3. Similar to N doping, the modification of P or S also helped to strengthen the surface acidity of CeO_2 and improved its catalytic reduction of NO_x, but phosphorus modification decreased the redox ability of catalyst.[23] Interestingly, the induced Ce^{4+}-SO_4^{2-} pair sites after sulfate modification could undermine the electronic interaction between SO_2 and CeO_2, thus improved the anti-SO_2 poisoning of CeO_2 catalyst by weakening the adsorption and oxidation of SO_2 on its surface.[24] At present, the gas-phase sulfation treatment of SO_2/CS_2 and the impregnation of sulfate/organic sulfur had been widely used to optimize and improve the NH_3-SCR performance of single CeO_2.[25] In our previous research, a novel sulfate modification with thiourea as the structure-directing agent had been proposed to improve the NH_3-SCR activity of CeO_2 catalyst synthesized by a one-pot hydrothermal method, and the results demonstrated that the introduction of thiourea not only regulated the morphology of CeO_2 catalyst, but also enhanced its acidity and surface oxygen vacancies, thus significantly improved the NH_3-SCR activity of catalyst.[26] In brief, the

catalytic performance of NO_x reduction over cerium oxide could be remarkably improved by the doping of Zr or sulfate modification through optimizing the surface acidity and redox properties of single CeO_2. However, the influence of Zr doping on the structure and de-nitrogen performance of the thiourea modified CeO_2 catalyst had been scarcely studied.

In this paper, a series of cerium-based catalysts were synthesized to investigate the promotional effect of Zr doping on the NH_3-SCR activity of CeO_2 and CeO_2-TA modified by thiourea during the hydrothermal treatment. We find that the doping of Zr contributes to improving the NH_3-SCR activity of both CeO_2 and CeO_2-TA catalysts, and $Ce_{0.95}Zr_{0.05}O_z$-TA exhibits the best catalytic performance of NO_x reduction. Furthermore, the morphology, crystal structure, pore structure, redox ability and surface acidity of the as-prepared catalysts were characterized via a series of experimental techniques, including X-ray diffraction (XRD), scanning electron microscopy (SEM), transmission electron microscopy (TEM), high-resolution transmission electron microscopy (HR-TEM), energy-dispersive X-ray spectroscopy (EDS), N_2 adsorption-desorption, Raman, X-ray photoelectron spectroscopy (XPS), Inductively coupled plasma(ICP), H_2 temperature-programmed reduction (H_2-TPR) and Pyridine infrared(Py-IR).

Results and discussion

Catalytic performance

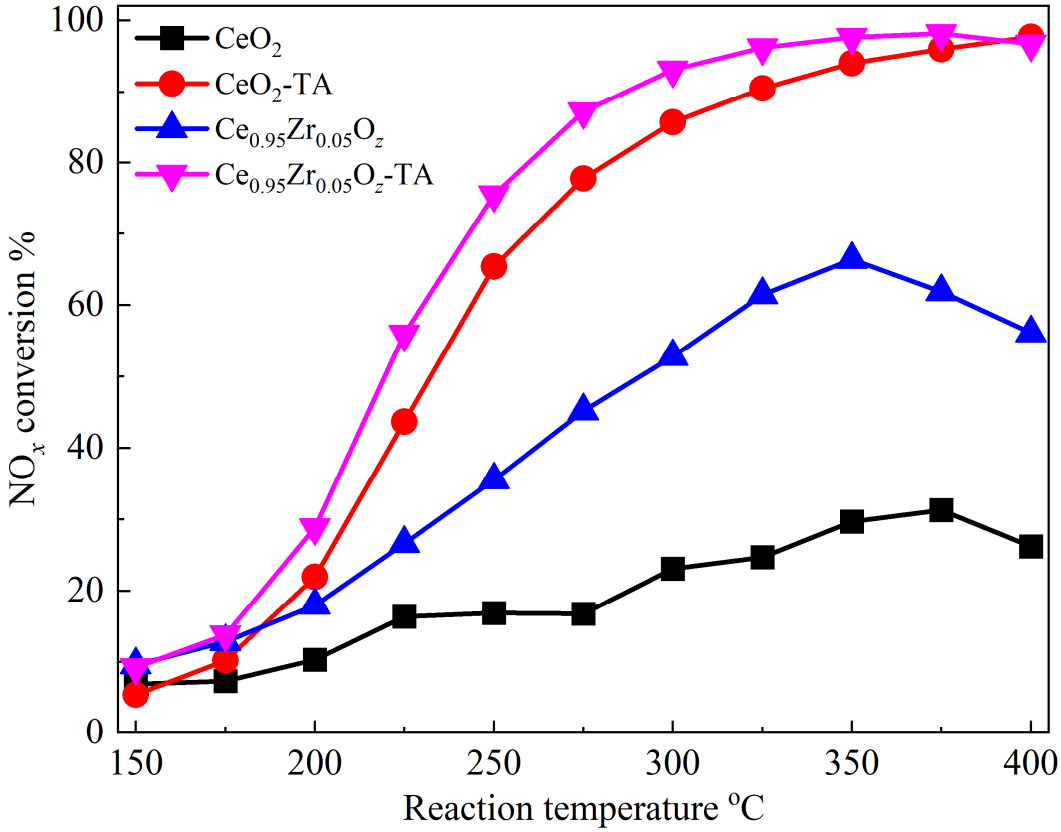

Figure 1. NO_x conversion of CeO_2, CeO_2-TA, $Ce_{0.95}Zr_{0.05}O_z$ and $Ce_{0.95}Zr_{0.05}O_z$-TA catalysts as a function of reaction temperature. Reaction conditions: [NH_3] = [NO] = 600 ppm, [O_2] = 5.0 vol.% and 1500 mL/min of total flow rate, 0.45 g of catalyst with the corresponding gas hourly space velocity (GHSV) of 200,000 mL/(g·h).

In our previous study, thiourea had been found to be a good structure-directing agent and sulfur source to optimize the NH_3-SCR activity of CeO_2 catalyst synthesized by a one-pot hydrothermal method, and the as-prepared CeO_2-TA catalyst presented the best NH_3-SCR activity when the molar ratio of thiourea/Cerium (TA/Ce) is 10.[26] Therefore, in order to further improve the NH_3-SCR activity of the above CeO_2-TA catalyst, zirconium has been introduced into and the influence of Zr doping molar ratio on the catalytic performance are given in Figure S1. From Figure S1, it can be

observed that when the doping molar ratio of Zr/(Ce+Zr) increases from 0.025 to 0.10, and the activity of $Ce_{1-x}Zr_xO_z$-TA catalyst firstly increases and then decreases and the suitable molar ratio of zirconium doping is 0.05. For comparison, we also investigated the effect of zirconium doping on the NH_3-SCR activity of CeO_2 by keeping the molar ratio of Zr/(Zr+Ce) being 0.05, and the results are given in Figure 1. The doping of Zr exactly improves the catalytic performance of CeO_2 greatly as expected, but the NO_x conversions of $Ce_{0.95}Zr_{0.05}O_z$ at 200~400 °C are still lower than those of CeO_2-TA, demonstrating that the modification of thiourea as the structure-directing agent and sulfur source presents better promotional effect on the NH_3-SCR activity of CeO_2 compared to Zr doping. Interestingly, $Ce_{0.95}Zr_{0.05}O_z$-TA exhibits the best catalytic performance of NO_x reduction at 200~400 °C among the tested four catalysts as shown in Figure 1. This indicates that there exists a synergistic promotional effect of Zr doping and thiourea modification on the NH_3-SCR activity of CeO_2. In order to better evaluate the catalytic performance of the as-prepared $Ce_{0.95}Zr_{0.05}O_z$-TA catalyst, the NO_x conversions over the reported commercial V-W(Mo)/Ti, Cu-CHA and Cu-SAPO-34 catalysts are summarized and shown in Table 1. It can be observed that under the high mass GHSV of 200,000 mL/(g·h), $Ce_{0.95}Zr_{0.05}O_z$-TA exhibits better NH_3-SCR performance than the commercial V-W(Mo)/Ti at the absence of SO_2 or/and H_2O. Meanwhile, compared with the new Cu-CHA catalyst, the hydrothermal stability and reactive temperature window of $Ce_{0.95}Zr_{0.05}O_z$-TA need to be further optimized.

The resistance to H_2O or/and SO_2 poisoning is crucial for the practical application of commercial or developed catalysts. Thus, the influence of Zr doping on the anti-H_2O/SO_2 poisoning of CeO_2-TA was measured at 300 °C. As shown in Figure S2, the introduction of 100 ppm SO_2 for 8 h could decrease the NO_x conversion of CeO_2-TA at 300 °C by 27%, but the further addition of

H_2O leads to a rapid reduction on the activity of catalyst. Furthermore, the NO_x conversion of CeO_2-TA does not return to the initial value when both SO_2 and H_2O have been cut off. This demonstrates that the CeO_2-TA catalyst shows poor anti-SO_2 or/and H_2O poisoning, and the doping of Zr improves its anti-SO_2 or/and H_2O poisoning, but the introduction of both SO_2 and H_2O also leads to the irreversible deactivation of NH_3-SCR activity for $Ce_{0.95}Zr_{0.05}O_z$-TA, which needs to be overcome before its practical application. In order to reveal the promotional influence of Zr doping on the NH_3-SCR activity of the thiourea modified cerium oxide catalyst, the as-prepared CeO_2, CeO_2-TA, $Ce_{0.95}Zr_{0.05}O_z$ and $Ce_{0.95}Zr_{0.05}O_z$-TA catalysts were chosen to be characterized for comparison.

Table 1. The summaries of catalytic activity over various commercial V-W(Mo)/Ti and reported catalysts.

Catalysts	NO_x conversion (%) at 200 °C	NO_x conversion (%) at 300 °C	Temperature window (°C) (X_{NO}>80%)	GHSV/MHSV	Reference
V_2O_5-WO_3/TiO_2	40-50	90-100	225-500	120,000 /h	[27]
V_2O_5-MoO_3/TiO_2	50	90-100	250-400	45,000 /h	[28]
V/WTi	20-30	80-90	300-450	18,000 /h	[29]
VWTi	10-20	80-90	300-500	75,000 /h	[30]
$V_{2.7}W_4Ti$	60-70	90-100	225-375	5,000 /h	[31]
Cu-CHA_{DNL}-DEA	90-100	90-100	175-550	300,000 /h	[32]
Cu-SSZ-13@CZO	40-50	90-100	250-500	60,000 /h	[10b]
Cu-SAPO-34(OP)	30-40	90-100	250-300	15,000 mL/(g·h)	[33]
$Ce_{0.95}Zr_{0.05}O_z$-TA	29	93	275-400	200,000 mL/(g·h)	In this work

XRD patterns

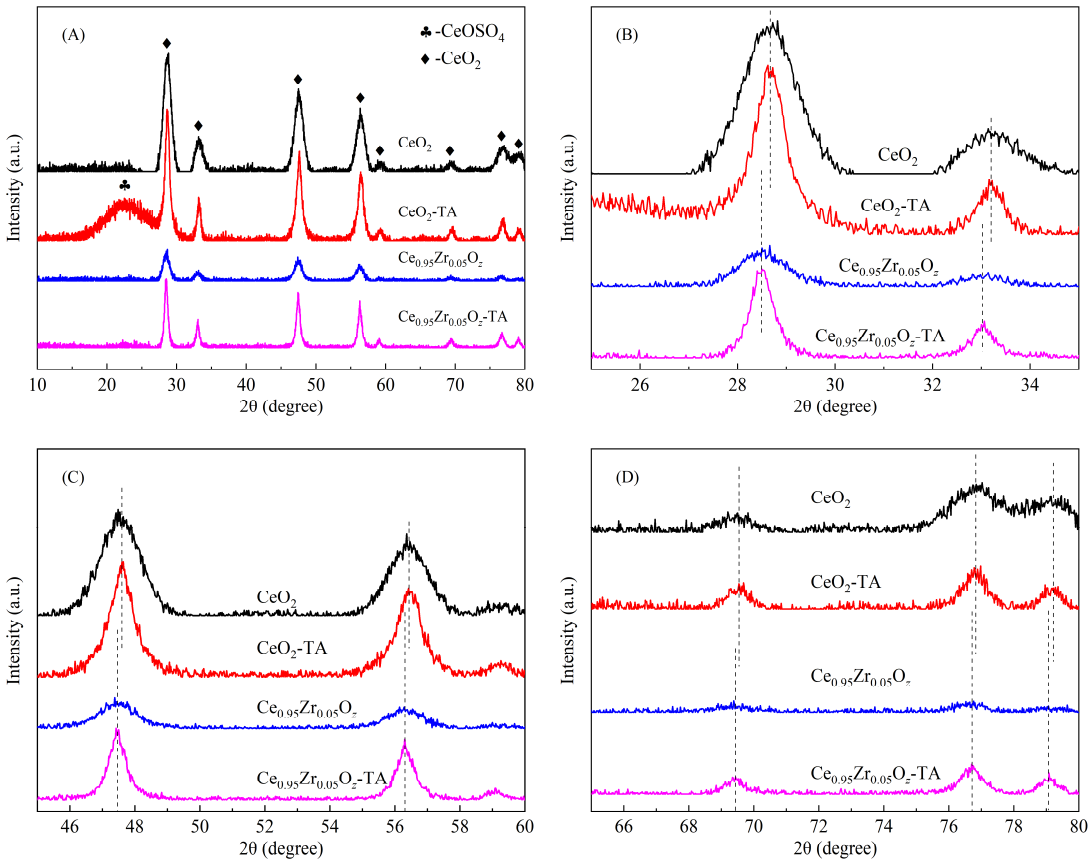

Figure 2. XRD patterns of the as-prepared CeO_2, CeO_2-TA, $Ce_{0.95}Zr_{0.05}O_z$ and $Ce_{0.95}Zr_{0.05}O_z$-TA catalysts: (A) overall view (B-D) local enlarged view

Figure 2 gives the XRD patterns of CeO_2, CeO_2-TA, $Ce_{0.95}Zr_{0.05}O_z$, $Ce_{0.95}Zr_{0.05}O_z$-TA catalysts. It can be observed that there exist the dominant phase of cubic fluorite CeO_2 (PDF: 34-0394) for all catalysts,[31] but the main lattice diffraction peak of CeO_2 catalyst is enhanced to a certain extent by thiourea modification with another peak appeared at about 23° over it, which could be attributed to the crystal of $CeOSO_4$ (PDF: 39-0515).[26] Interestingly, the doping of zirconium weakens the intensity of diffraction peaks attributed to cubic fluorite CeO_2 for both CeO_2 and CeO_2-TA catalysts, and $Ce_{0.95}Zr_{0.05}O_2$ seems to have lost all the crystallinity attributed to cubic fluorite CeO_2, and the main reason for this phenomenon might be that the doped Zr ions get into the cubic fluorite CeO_2

crystal and induce the formation of Ce-Zr solid solution. Previous research confirmed this effect of Zr doping on the diffraction peaks of cubic fluorite CeO_2 in the nanorod CeO_2-NR support due to the incorporation of Zr^{4+} [18]. Zhou et al.[35] also found that the as-prepared Pd/$Ce_{0.8}Zr_{0.2}O_2$ catalyst presented weaker diffraction peaks of cubic fluorite CeO_2 than Pd/CeO_2, and its XRD pattern was analogous to that of CeO_2 due to the formation of homogeneous Ce-Zr solid solutions with a stable fluorite structure in it. However, the doping of Zr suppresses the formation of highly crystalline $CeOSO_4$ crystal even if thiourea had been added as the modified agent, suggesting that the induced S species are highly dispersed on the surface of $Ce_{0.95}Zr_{0.05}O_2$ or their particle sizes are too small to reach the detection limit of the detection instrument. Furthermore, the doping of zirconium makes the diffraction peaks attributed to cubic fluorite CeO_2 for both CeO_2 and CeO_2-TA catalysts shift slightly to lower angles, and enlarges the lattice parameter of cubic fluorite CeO_2 as shown in Table 2. Ma et al.[19] had pointed out that the doped Zr ions could mainly substitute on Ce sites of $Ce_{1-x}Zr_xO_2$ when the molar ratio of Zr/Ce was less than 0.06, thus induced dramatic structural distortion and led to lattice expansion. It should be mentioned that no diffraction peaks belonged to zirconium oxide had been detected in both $Ce_{0.95}Zr_{0.05}O_z$ and $Ce_{0.95}Zr_{0.05}O_z$-TA, which might be ascribed to a high dispersion of zirconia crystal. Therefore, it can be inferred that the doped Zr ions might enter into the CeO_2 matrix successfully and thereby induce the formation of highly dispersive Ce-Zr solid solution. But the presence of thiourea partially depresses these effect of Zr doping.

Table 2. The physical structural parameters of the CeO_2, CeO_2-TA, $Ce_{0.95}Zr_{0.05}O_z$ and $Ce_{0.95}Zr_{0.05}O_z$-TA catalysts

Samples	S_{BET}[a] (m^2/g)	Pore volume[b] (cm^3/g)	Average pore size[c] (nm)	Average crystallite size[d] (nm)	Lattice parameter[d] (nm)

CeO_2	119.62	0.199	6.44	10.3	0.540
CeO_2-TA	61.87	0.068	4.41	14.7	0.539
$Ce_{0.95}Zr_{0.05}O_z$	109.67	0.253	8.00	11.7	0.543
$Ce_{0.95}Zr_{0.05}O_z$-TA	50.96	0.122	7.71	17.6	0.542

[a] BET surface area

[b] BJH desorption pore volume

[c] BJH desorption pore diameter

[d] Calculated by Scherrer formula [35]

N_2 adsorption-desorption

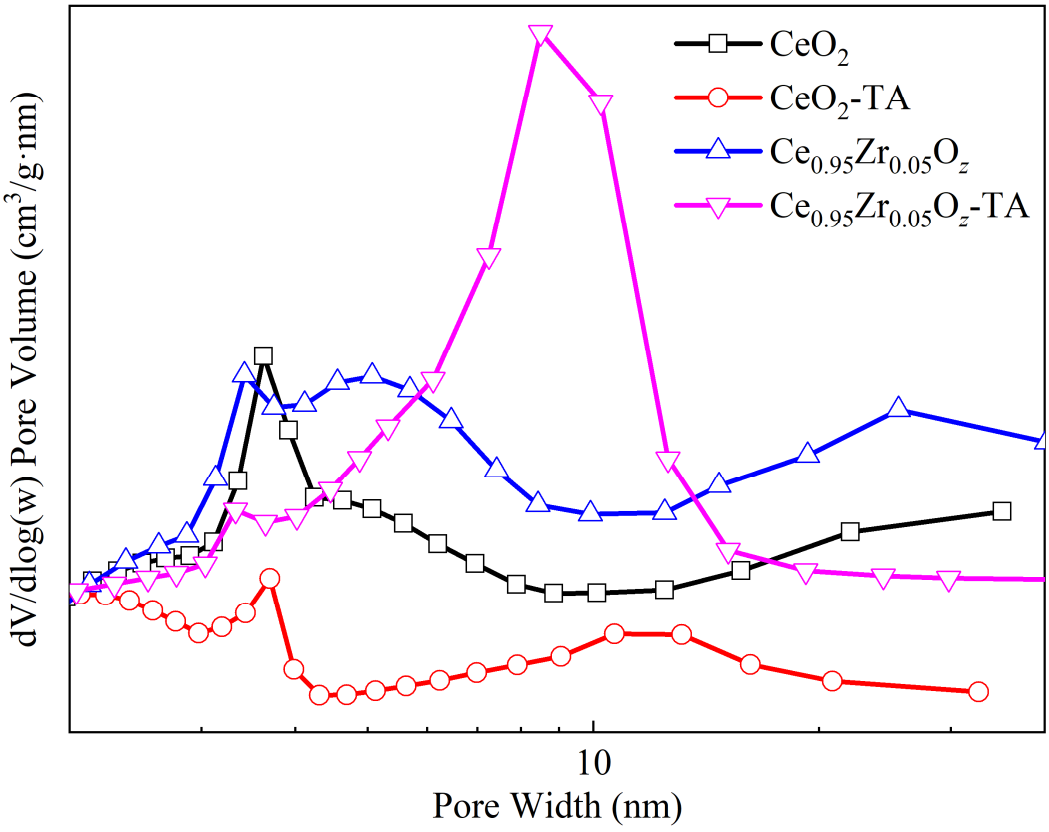

Figure 3. The pore size distributions of CeO_2, CeO_2-TA, $Ce_{0.95}Zr_{0.05}O_z$ and $Ce_{0.95}Zr_{0.05}O_z$-TA catalysts.

The N_2 adsorption-desorption analysis was performed to investigate the influence of Zr doping

on the pore structure of CeO_2 and CeO_2-TA catalysts. It can be observed from Figure S3 that the CeO_2, CeO_2-TA, $Ce_{0.95}Zr_{0.05}O_z$ and $Ce_{0.95}Zr_{0.05}O_z$-TA catalysts all exhibit typical type-IV N_2 adsorption-desorption isotherms, wherein exists different hysteresis loops. According to IUPAC classification, the N_2 adsorption-desorption isotherms of CeO_2, CeO_2-TA and $Ce_{0.95}Zr_{0.05}O_z$ can be attributed to type-H3, suggesting the meso-porous structure due to the accumulation of particles.[37] Meanwhile, the hysteresis loop of $Ce_{0.95}Zr_{0.05}O_z$-TA is assigned to type-H2, demonstrating the "ink bottle" meso-porous. Furthermore, the thiourea modification or Zr doping doesn't change the low-pressure closing point of the N_2 adsorption-desorption isotherm of CeO_2 catalyst, but the doping of Zr contributes to improving its pore volume unlike the inhibition of thiourea modification. Unfortunately, the synchronous addition of thiourea and Zr doping leads to the collapse of partial meso-porous of CeO_2 catalyst, and make its low-pressure closing point shift to right. As shown in Figure 3, different from the adverse effect of thiourea modification, the doping of Zr enlarges the pore size distribution of CeO_2 catalyst, especially promotes the formation of meso-porous at 4~40 nm. However, the synchronous addition of thiourea and Zr doping is disadvantageous to the formation of meso-porous at 2~4 nm, and lead to more concentrated meso-pore distribution for $Ce_{0.95}Zr_{0.05}O_z$-TA. According to the calculated results of BET surface areas and pore volumes in Table 2, we can find that CeO_2 presents the largest BET surface area and the specific surface areas of catalysts decrease as follows: CeO_2>$Ce_{0.95}Zr_{0.05}O_z$>CeO_2-TA>$Ce_{0.95}Zr_{0.05}O_z$-TA, and the doping of Zr decreases the BET surface area of CeO_2 from 119.62 m^2/g to 109.67 m^2/g. But the modification of thiourea effectively reduces the specific surface areas of both CeO_2 and $Ce_{0.95}Zr_{0.05}O_z$ due to collapse of partial mesoporous,[26] and the decreased effect of Zr doping on the surface area of CeO_2 had also been found by previous study when the doping molar ratio of Zr/Ce was low [20]. Generally,

larger BET surface area or/and a broad pore size distribution usually has been thought to be the important reasons for better NH_3-SCR activity of catalyst.[38] However, according to the results in Figure 1, the CeO_2 catalyst of the maximum specific surface area presents the worst catalytic performance, but $Ce_{0.95}Zr_{0.05}O_z$-TA exhibits the best NH_3-SCR activity with the minimum specific surface area and the most concentrated pore size distribution. Therefore, the larger surface area or a broad pore size distribution might not be a key factor affecting the NH_3-SCR activity of the above as-prepared Ce-based catalysts.

SEM, TEM/HR-TEM and EDS characterization

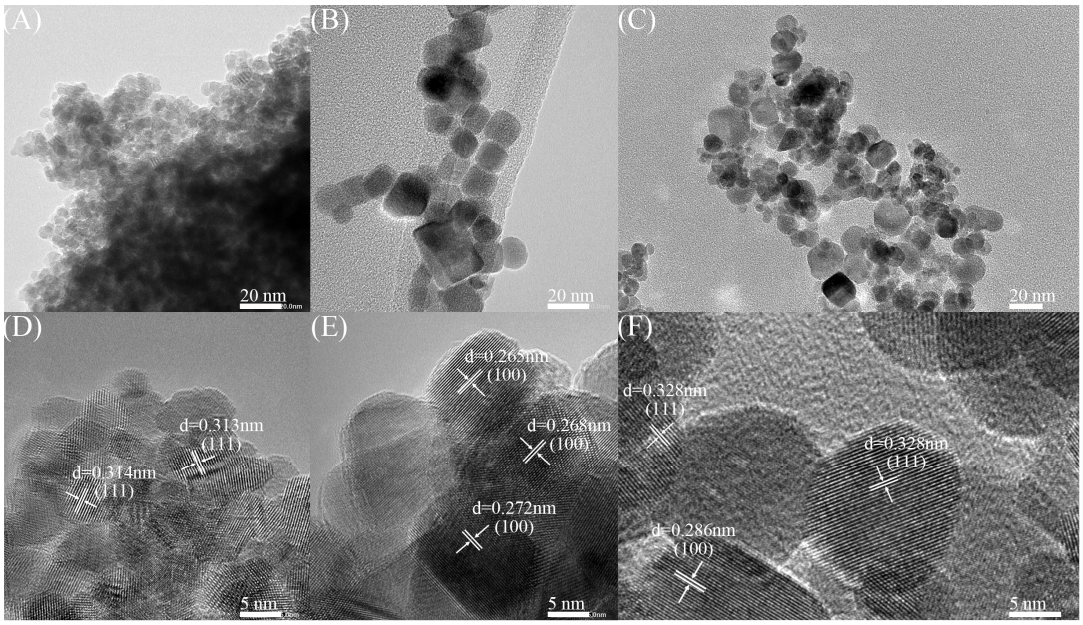

Figure 4. TEM images and HR-TEM images of CeO_2 (A, D), CeO_2-TA (B, E) and $Ce_{0.95}Zr_{0.05}O_z$-TA (C, F) catalysts.

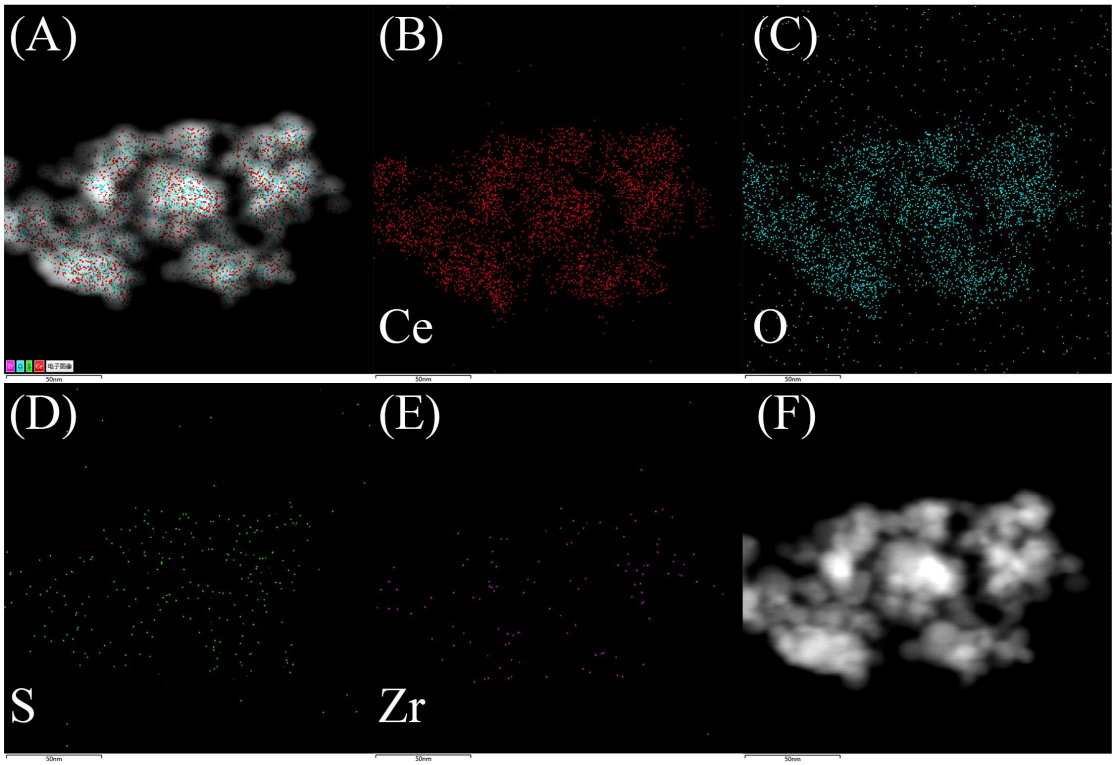

Figure 5. The elemental mapping images of $Ce_{0.95}Zr_{0.05}O_z$-TA catalyst.

In order to investigate the surface morphology, the SEM measurements were performed and the SEM images of CeO_2, CeO_2-TA, $Ce_{0.95}Zr_{0.05}O_z$ and $Ce_{0.95}Zr_{0.05}O_z$-TA catalysts are shown in Figure S4. It can be observed from Figure S4 that all samples compose of nanoparticles with a certain degree of agglomeration. Among them, CeO_2 exhibits the bulk morphology composed of small and regular particles, while CeO_2-TA shows a larger bulk morphology composed of larger particles. Interestingly, the doping of Zr decreases the crystallization and agglomeration of CeO_2 and CeO_2-TA, Both $Ce_{0.95}Zr_{0.05}O_z$ and $Ce_{0.95}Zr_{0.05}O_z$-TA present the loose morphology, but the latter is composed of regular and refined particles. To obtain more detailed information, TEM/HR-TEM were performed. According to the results of TEM/HR-TEM in Figure 4, it can be found that the modification of thiourea not only regulates the exposed facets from (111) (Inter-planar Spacing, 0.313 nm) to (100) (Inter-planar Spacing, 0.268 nm) for the formed cubic fluorite CeO_2, but also makes its morphology transform from nanoparticles to nanocubes.[39] Furthermore, the results of the

calculated corresponding particle size distribution in Figure S5 demonstrate that the modification of thiourea enlarges the particle size of CeO_2 catalyst. However, Zr doping can partially restrain the regulation of thiourea modification on the surface morphology of the formed cubic fluorite CeO_2, and $Ce_{0.95}Zr_{0.05}O_z$-TA displays an irregular morphology composed of both nanoparticles and nanocubes in a wide range of sizes from about 6 to 24 nm. Previous study indicated that the doping of Zr contributed to the exposing of (111) and (100) facets and led to the expansion of the lattice of cubic fluorite CeO_2.[40] Interestingly, $Ce_{0.95}Zr_{0.05}O_z$-TA presents two exposed facets of (111) and (100) with larger inter-planar spacing (0.328 nm and 0.287 nm) than those of both CeO_2 and CeO_2-TA.[41] This demonstrates that the doping of Zr also helps to the lattice expansion of cubic fluorite CeO_2 via increasing its inter-planar spacings even if thiourea was used as the modified agent, which is in accordance with the XRD results in Figure 2. Furthermore, in order to investigate the dispersion of composition elements, the elemental mapping images of $Ce_{0.95}Zr_{0.05}O_z$-TA are measured and it can be found that the thiourea modification and zirconium doping contributes to the formation of highly dispersive S and Zr species on the surface of CeO_2, which is consistent with the XRD results in Fig.2.

Raman spectroscopic characterization

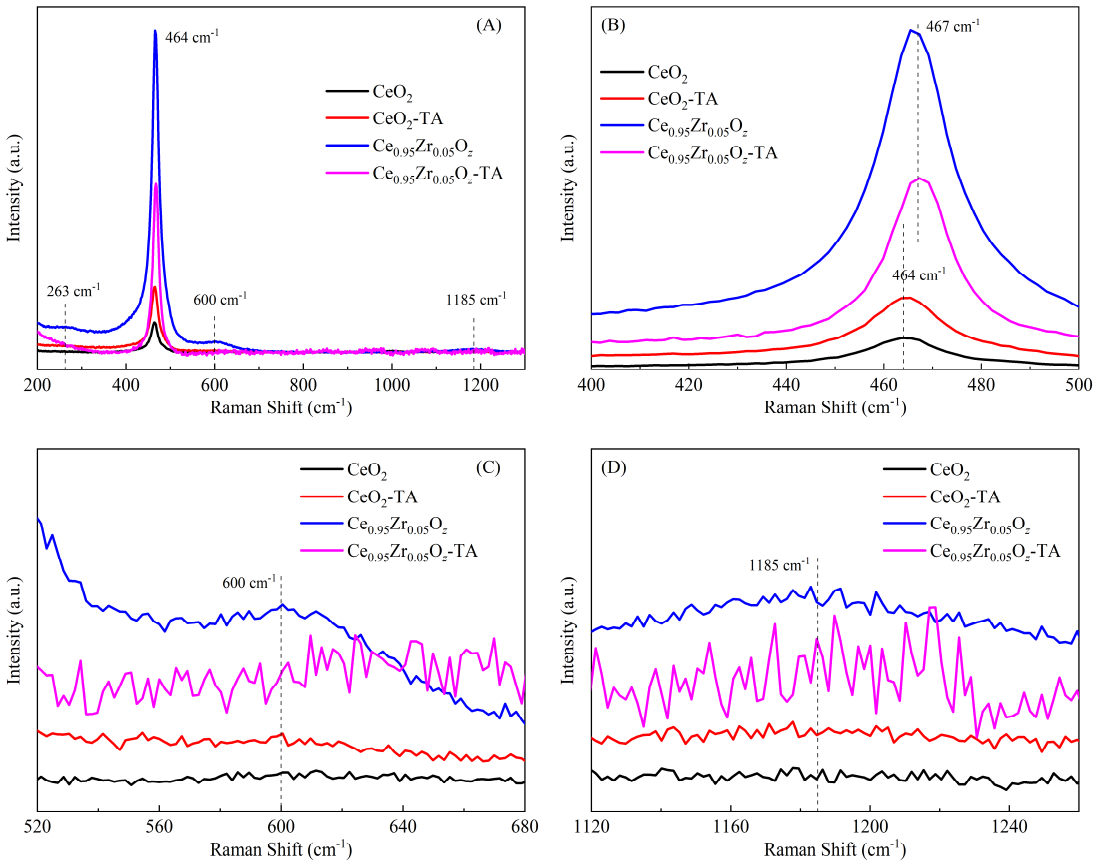

Figure 6. The Raman spectra of CeO_2, CeO_2-TA, $Ce_{0.95}Zr_{0.05}O_z$ and $Ce_{0.95}Zr_{0.05}O_z$-TA catalysts (A) overall view (B-D) local enlarged view.

Figure 6(A) gives the Raman spectra of CeO_2, CeO_2-TA, $Ce_{0.95}Zr_{0.05}O_z$ and $Ce_{0.95}Zr_{0.05}O_z$-TA catalysts and four peaks can be observed over samples. Among them, the peak located at 263 cm^{-1} is assigned to the second-order transverse acoustic (2TA) mode of CeO_2 or the disorder in the system,[42] while the strong peak located at 464 cm^{-1} is attributed to the F_{2g} vibration mode of cubic fluorite CeO_2.[43] According to the enlarged Raman shift results of 400~500 cm^{-1}, we can find that Zr doping not only exhibits stronger enhancement on the intensity of the F_{2g} vibration mode of the symmetric breathing mode of oxygen atoms around cerium ions in cubic fluorite CeO_2 than thiourea modification, but also leads the F_{2g} bands of both CeO_2 and CeO_2-TA shift from 464 cm^{-1} to 467 cm^{-}

[1], attributing to the influence of Zr doping on the variation of interatomic force in CeO_2 crystal and the enlargement of crystal size, which are in consistent with the XRD results.[44]

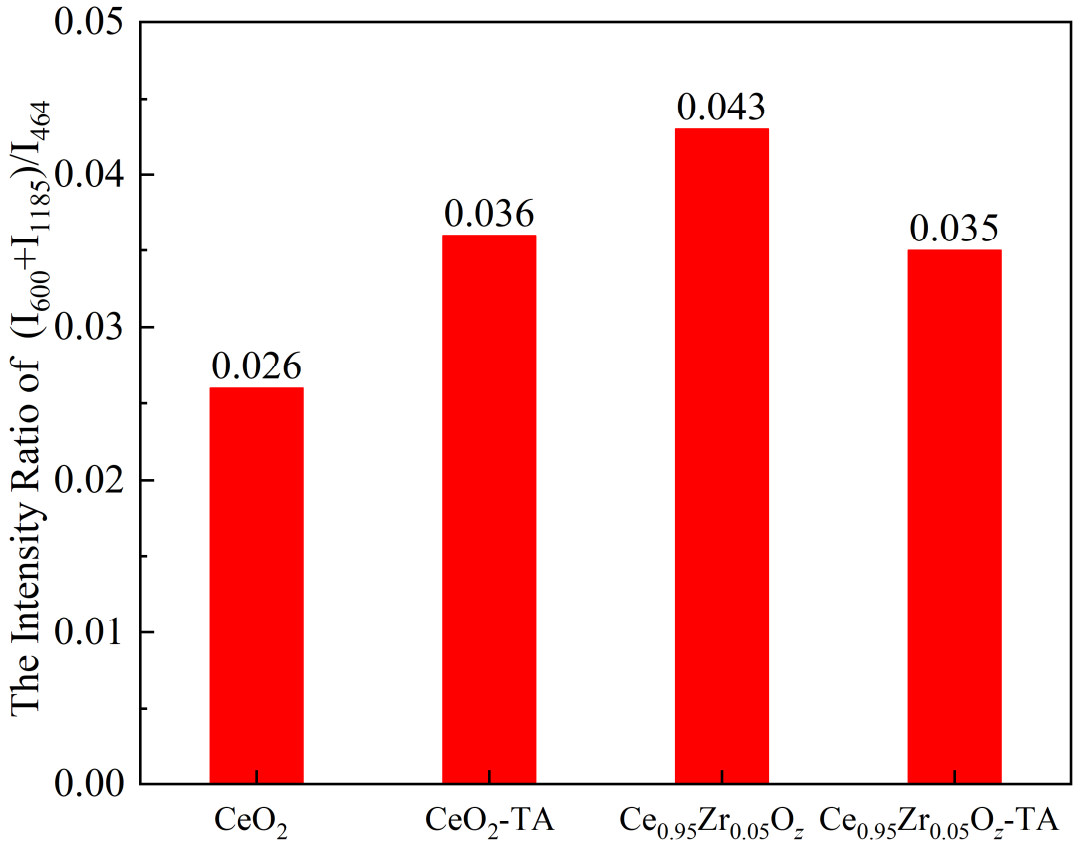

Figure 7. The corresponding peak intensity ratio of $(I_{600}+I_{1180})/I_{464}$ over the as-prepared CeO_2, CeO_2-TA, $Ce_{0.95}Zr_{0.05}O_z$ and $Ce_{0.95}Zr_{0.05}O_z$-TA catalysts.

Previous study pointed out that the generation of oxygen vacancy could accelerate the mobility of active oxygen, thereby facilitated the NH_3-SCR reaction of catalyst. Simultaneously, the detected Raman bands at about 600 cm^{-1} and 1185 cm^{-1} were usually attributed to the surface oxygen defects.[45] Thus, the relative peak intensity ratio of $(I_{600}+I_{1185})/I_{464}$ was calculated to investigate the influence of thiourea modification and Zr doping on the concentration of oxygen vacancies or/and defects. As shown in Figure 7, both thiourea modification and Zr doping promote the generation of oxygen defects and vacancies of CeO_2 catalyst due to the charge imbalance and the lattice distortion

of cubic fluorite CeO_2 brought by non-metal and metal ions doping.[46] However, $Ce_{0.95}Zr_{0.05}O_z$ exhibits the highest $(I_{600}+I_{1185})/I_{464}$ ratio, and the calculated value of $Ce_{0.95}Zr_{0.05}O_z$-TA is even lower than that of CeO_2-TA.

Surface chemical properties and catalyst composition

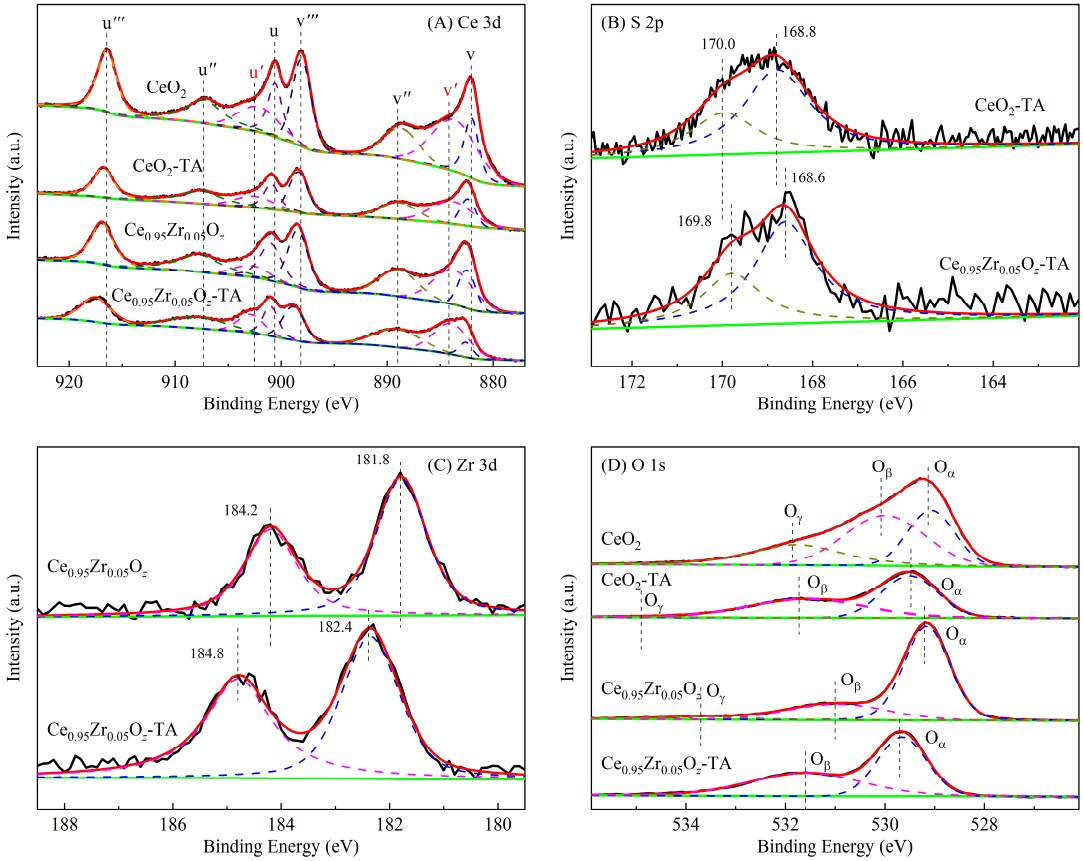

Figure 8. The XPS spectra of CeO_2, CeO_2-TA, $Ce_{0.95}Zr_{0.05}O_z$ and $Ce_{0.95}Zr_{0.05}O_z$-TA catalysts: (A) Ce 3d, (B) S 2p, (C) Zr 3d, (D) O 1s.

The XPS measurements were performed to investigate the influence of Zr doping on the concentration of elements and their valence states on the surface of CeO_2 and CeO_2-TA catalysts. According to the results in Figure 8(A), it can be found that there exist both Ce^{3+} (u' and v') and Ce^{4+} (u, u'', u''', v, v'' and v''') species on all catalysts surface by de-convoluting the Ce 3d spectra into eight peaks using Gaussian Lorentzian profiles.[47] Meanwhile, the existence of Ce^{3+} species

has been usually thought to promote the generation of oxygen vacancies, charge imbalance and unsaturated chemical bands, which contribute to enhancing the adsorption of NH_3 and the catalytic oxidization of NO to NO_2, thereby helps to improve the NH_3-SCR activity of Ce-based catalyst.[48] Therefore, the surface molar ratio of $Ce^{3+}/(Ce^{3+}+Ce^{4+})$ of samples were calculated using the followed equation, and S represents the integrated area of the corresponding peak herein.

$$Ce^{3+}(\%)=\frac{S_{u'}+S_{v'}}{\sum(S_u+S_v)}\times 100 \quad (2)$$

As shown in Table 3 and Table 4, thiourea modification decreases the relative concentration of Ce^{3+} species on the surface of CeO_2 and its surface $Ce^{3+}/(Ce^{3+}+Ce^{4+})$ molar ratio, which might be attributed to the formation of $CeOSO_4$.[26] In addition, the doping of Zr increases the relative concentrations of Ce^{4+} and total Ce species, and presents stronger lowering effect on the surface $Ce^{3+}/(Ce^{3+}+Ce^{4+})$ molar ratio compared to thiourea modification. Interestingly, $Ce_{0.95}Zr_{0.05}O_z$-TA exhibits higher $Ce^{3+}/(Ce^{3+}+Ce^{4+})$ molar ratio than those of CeO_2-TA and $Ce_{0.95}Zr_{0.05}O_z$ due to the decrease of surface Ce^{4+} under the joint action of thiourea modification and Zr doping. Furthermore, Zr doping makes the Binding Energy of S^{6+} species on the surface of CeO_2-TA shift to left, and thiourea modification presents a similar effect on the Binding Energy of Zr^{4+} species on the surface of $Ce_{0.95}Zr_{0.05}O_z$. Previous study revealed that sulfur centers could intensively withdraw electrons, and increased the electron cloud density around S, which led to the generation of electron-defect site centered at Zr and decreased the electron cloud density of Zr due to the interaction between S and Zr species.[50] Therefore, it might be deduced that there exists the electronic interaction of the introduced Zr and S species in $Ce_{0.95}Zr_{0.05}O_z$-TA, thus leads to the shift of their Binding energies.[51]

Table 3. Surface composition and atomic ratios of the as-prepared catalysts calculated from XPS.

Catalysts	Atomic concentrations (%)				Atomic ratios (%)	
	Ce	Zr	O	S	$Ce^{3+}/(Ce^{3+}+Ce^{4+})$	$O_\beta/(O_\alpha+O_\beta+O_\gamma)$
CeO_2	36.16	-	63.84	-	31.34	44.16
CeO_2-TA	33.13	-	62.39	4.48	26.27	48.43
$Ce_{0.95}Zr_{0.05}O_z$	36.27	1.66	62.07	-	22.62	24.69
$Ce_{0.95}Zr_{0.05}O_z$-TA	28.54	2.69	64.42	4.35	29.26	49.27

According to the results in Figure 8(D) and Table 3, the O 1s XPS spectra of catalysts can be fitted into three peaks using Gaussian Lorentzian profiles, which are assigned to the lattice oxygen in CeO_2 (Denoted as O_α, Located at about 529 eV), the surface chemisorbed oxygen (Denoted as O_β, Located at about 530 eV) and the lattice oxygen ions in Ce_2O_3 (Denoted as O_γ, Located at about 532 eV),[52] respectively. Both thiourea modification and Zr doping enlarge the binding energy of O 1s for CeO_2 catalyst because of the lower electron cloud density of O species induced by the introduction of S or/and Zr ions.[53] Due to the stronger migration ability and higher reactivity, the surface chemisorbed oxygen(O_β) has usually been thought to improve the low-medium temperature NH_3-SCR activity of catalyst by increasing its catalytic oxidization of NO to NO_2 via the “fast-SCR” reaction.[48] Thus, the surface molar ratios of $O_\beta/(O_\alpha+O_\beta+O_\gamma)$ were also calculated herein. As shown in Tables 3 and 4, thiourea modification increases the $O_\beta/(O_\alpha+O_\beta+O_\gamma)$ molar ratio on CeO_2 catalyst surface due to the formation of sulfate species.[54] Furthermore, the further thiourea modification induces highly dispersive sulfate species formed on the surface of $Ce_{0.95}Zr_{0.05}O_z$, and increases the relative concentrations of both Ce^{3+} and Zr^{4+} with its surface Ce^{4+} species decreasing.[46] However, the Raman results indicate that $Ce_{0.95}Zr_{0.05}O_z$ has the most oxygen defect and presents the best low-

temperature H_2-reduction according to the following H_2-TPR spectra, which are obviously inconsistent with the calculated surface $O_\beta/(O_\alpha+O_\beta+O_\gamma)$ molar ratios. Therefore, the relative concentration of O_β from XPS might not correlate with the NH_3-SCR activity correctly. For example, Yao et al.[18] had found that Zr doping enriched the oxygen defect of MnO_x/CeO_2 nano-rod catalyst, but it inhibited the generation of surface adsorption oxygen(O_β).

Table 4. Surface atomic concentration of the as-prepared catalysts calculated from XPS.

Catalysts	Surface atomic concentration (%)						
	Ce^{3+}	Ce^{4+}	Zr^{4+}	S^{6+}	O_α	O_β	O_γ
CeO_2	11.33	24.83	-	-	18.36	28.19	17.29
CeO_2-TA	8.70	24.43	-	4.48	31.21	30.21	0.96
$Ce_{0.95}Zr_{0.05}O_z$	8.20	28.07	1.66	-	43.06	15.33	3.68
$Ce_{0.95}Zr_{0.05}O_z$-TA	8.35	20.19	2.69	4.35	32.68	31.74	-

In order to further investigate the influence of thiourea modification and Zr doping on the actual composition of CeO_2, the ICP measurement was performed and the results are given in Table 5. It can be found that the modification of thiourea decreases the content of Ce element of CeO_2, which might be attributed to the formed sulfate in catalyst. However, the doping of Zr scarcely affect the contents of Ce element for both CeO_2 and CeO_2-TA catalysts. According to the tested data of ICP, the calculated molar ratio of Zr/Ce is 0.0474 for $Ce_{0.95}Zr_{0.05}O_z$, while this value of $Ce_{0.95}Zr_{0.05}O_z$-TA is 0.0614. Therefore, it can be deduced that the introduction of thiourea or zirconium might influence the crystallite and formation of cubic fluorite CeO_2, thus regulates the actual composition for the as-prepared CeO_2-TA, $Ce_{0.95}Zr_{0.05}O_z$ and $Ce_{0.95}Zr_{0.05}O_z$-TA catalysts.

Table 5. The element contents of the as-prepared catalysts calculated from ICP.

Samples	Element contents of catalysts (mmol/g)		
	Ce	Zr	S
CeO_2	5.03	-	-
CeO_2-TA	4.76	-	0.21
$Ce_{0.95}Zr_{0.05}O_z$	5.02	0.25	-
$Ce_{0.95}Zr_{0.05}O_z$-TA	4.74	0.31	0.16

The properties of redox ability

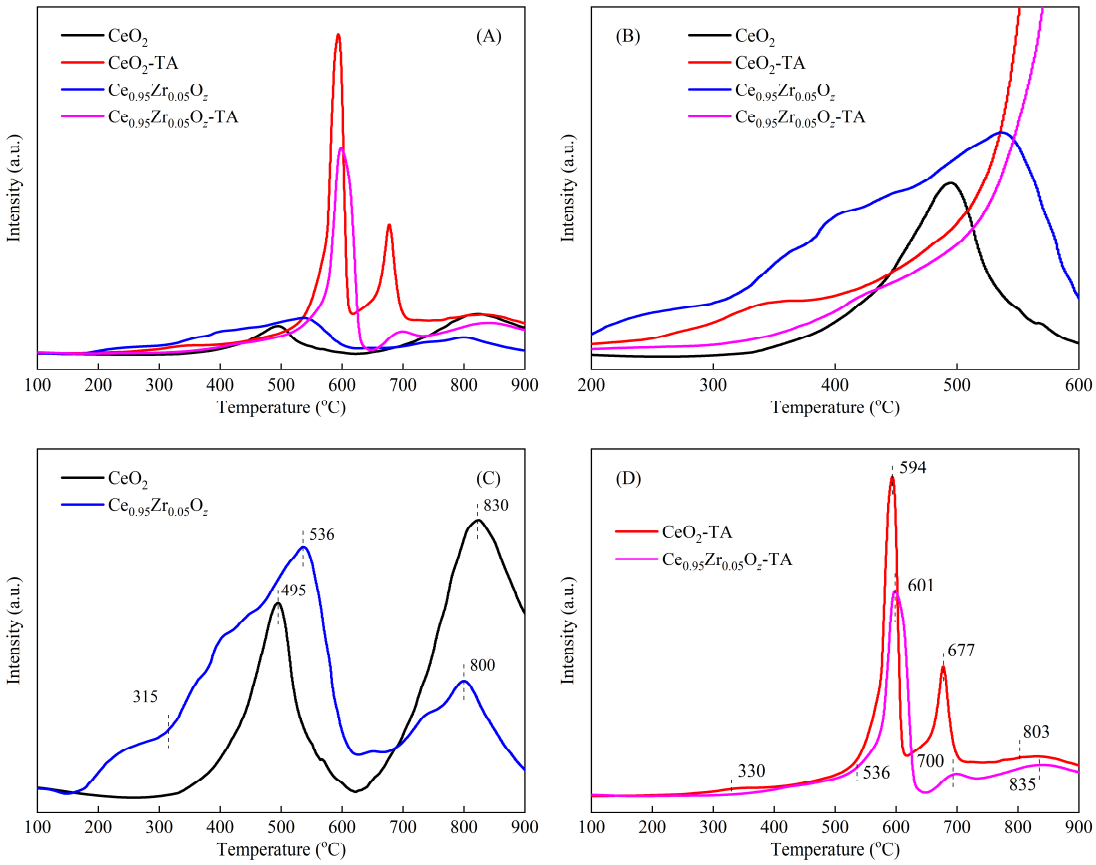

Figure 9. The H_2-TPR profiles of the as-prepared CeO_2, CeO_2-TA, $Ce_{0.95}Zr_{0.05}O_z$ and $Ce_{0.95}Zr_{0.05}O_z$-TA catalysts.

Generally, the redox activity has been recognized as another crucial influencing factor on the NH_3-SCR activity of catalyst.[55] Thus, the effect of Zr doping on the redox properties of CeO_2 and

CeO_2-TA catalysts were characterized by H_2-TPR, and the results are given in Figure 9. Some previous studies pointed out that there existed three H_2-TPR peaks for CeO_2, located at about 200~430 °C, 430~600 °C and above 700 °C, which could be attributed to the reduction of surface absorbed oxygen, deeper interior nanoparticles oxygen and bulk lattice oxygen, respectively.[56] However, Yu et al.[57] and Wu et al.[58] had attributed the H_2-TPR peaks of CeO_2 to the reduction of the surface/sub-surface lattice oxygen, deeper interior nanoparticles oxygen and bulk lattice oxygen from 200 °C to 900 °C. According to the results in Figure 9, it can be found that the as-prepared CeO_2 catalyst presents two obvious reduction peaks with the peak positions being 495 °C and 830 °C, mainly ascribed to the H_2-reduction of deeper interior nanoparticles oxygen and bulk lattice oxygen, respectively. Different from the promotional effect of thiourea modification on the H_2-reduction intensity of CeO_2 at 500~900 °C, the doping of Zr increases its reducibility below 600 °C, indicating a stronger effect on promoting the formation of surface absorbed oxygen or surface/sub-surface lattice oxygen and the reducibility of nanoparticles oxygen due to the formation of Ce-Zr solid solution.[16] Unfortunately, $Ce_{0.95}Zr_{0.05}O_z$-TA presents the weakest H_2-reduction intensity below 500 °C compared to the other three catalysts, indicating that it has the least surface adsorbed oxygen or/and surface/sub-surface lattice oxygen, which is obviously inconsistent with the calculation results of XPS. It should be mentioned that the doping of Zr leads to the disappearance of reduction peak attributed to $CeOSO_4$ for CeO_2-TA [59], but $Ce_{0.95}Zr_{0.05}O_z$-TA also exhibits a strong reduction peak between the two reduction peaks of 594 °C and 677 °C of CeO_2-TA, which are mainly attributed to the reduction of nanoparticles oxygen or/and highly dispersive sulfate species.[53b] Previous studies demonstrated that the doping of Zr increased the reducibility of Ce-based catalyst and improved the H_2-reduction temperature of the formed sulfate species via the gas phase sulfation

pretreatment.[46,56a] Therefore, the doping of Zr contributes to the formation of Ce-Zr solid solution and induces the highly dispersive sulfate species rather than the high crystallinity $CeOSO_4$ crystal when thiourea had been used as the modified agent. But $Ce_{0.95}Zr_{0.05}O_z$-TA presents the least surface adsorbed oxygen or/and surface/sub-surface lattice oxygen according to the H_2-TPR results, which is inconsistent/correlated with the XPS results/the activity in Figure 1.

Py-IR

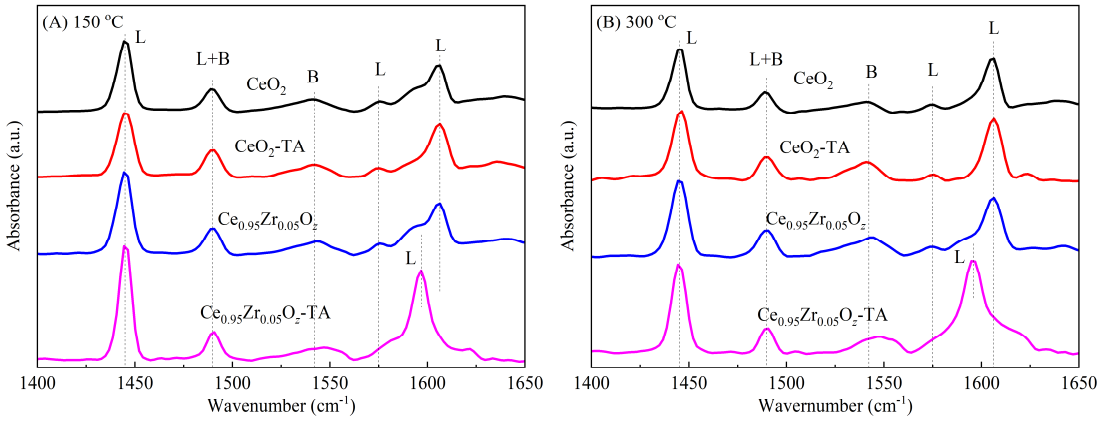

Figure 10. The Py-IR curves of CeO_2, CeO_2-TA, $Ce_{0.95}Zr_{0.05}O_z$ and $Ce_{0.95}Zr_{0.05}O_z$-TA catalysts.

To investigate the Lewis and Brønsted acid sites of the as-prepared catalysts, Py-IR was performed and the corresponding results are shown in Figure 10. The Py-IR curves at 150 °C and 300 °C for the samples are attributed to the weak acid sites and medium-strong acid sites, respectively. Several Py-IR peaks can be found and the peak located at about 1542 cm^{-1} is assigned to the C-N stretching of pyridine adsorbed to the Brønsted acid sites.[60] The peaks at about 1445 cm^{-1}, 1575 cm^{-1}, 1597 cm^{-1}, and 1606 cm^{-1} are attributed to Lewis acid sites.[61] In addition, the peak at about 1490 cm^{-1} is due to the interaction of pyridine molecules with both Brønsted and Lewis acid sites.[62] In order to further explore the influence of thiourea modification and Zr doping on the acid sites of CeO_2 catalyst, the quantitative amounts of Lewis and Brønsted acid sites were calculated according to the Py-IR curves at 150 °C and 300 °C and the results are shown in Table 6.

It can be observed that thiourea modification reduces the weak Brønsted acid sites of CeO_2 catalyst but increases its medium-strong Brønsted and Lewis acid sites. In addition, Zr doping increases the weak and medium-strong acid, including Brønsted and Lewis acid sites. Furthermore, $Ce_{0.95}Zr_{0.05}O_z$-TA presents a strong Py-IR peak at about 1597 cm^{-1} attributed to Lewis acid sites. This demonstrates that thiourea modification and Zr doping exhibit a synergistic promotional effect on optimizing Lewis acid sites of CeO_2, and $Ce_{0.95}Zr_{0.05}O_z$-TA shows the highest amount of both weak and medium-strong Lewis acid sites, which might be an important reason for its better NH_3-SCR activity.

Table 6. Concentration and distribution of Lewis (L) and Brønsted (B) acid sites on the investigated catalysts.

Catalysts	Weak acid (μmol/g)			Medium-strong acid (μmol/g)		
	B	L	B/L	B	L	B/L
CeO_2	19.00	32.53	0.584	7.21	11.78	0.612
CeO_2-TA	15.56	32.46	0.479	9.29	13.57	0.685
$Ce_{0.95}Zr_{0.05}O_z$	21.28	39.60	0.537	11.56	17.84	0.648
$Ce_{0.95}Zr_{0.05}O_z$-TA	21.07	45.38	0.464	9.51	18.03	0.527

Conclusions

In this paper, thiourea modification and Zr doping were used to optimize the NH_3-SCR activity of CeO_2 catalyst for comparison, and they present a synergistic promotional effect on the activity of catalyst. Unlike the influence of thiourea modification on promoting the agglomeration of the as-prepared CeO_2 nanoparticles, the transformation of catalyst morphology from nanoparticles to nanocubes and the formation of high crystallinity $CeOSO_4$ crystal, the doping of Zr lowers the agglomeration of the CeO_2 nanoparticles, loosens the surface morphology of catalyst and promotes

the formation of Ce-Zr solid solution. This induces the highly dispersive cerium/zirconium sulfate species formed on the surface of $Ce_{0.95}Zr_{0.05}O_z$-TA rather than the high crystallinity $CeOSO_4$ crystal when thiourea was also introduced as the modified agent, and $Ce_{0.95}Zr_{0.05}O_z$-TA presents an irregular morphology composed of both nanoparticles and nanocubes with the minimum specific surface area and most concentrated pore size distribution. Furthermore, thiourea modification and Zr doping exhibit a synergistic promotional effect on the dispersion of Ce^{3+} and S^{6+} species on the surface of catalyst, and increase the concentrations of its surface total oxygen (O_{total}) and chemisorbed oxygen (O_β). Interestingly, different from the promotional effect of thiourea modification or Zr doping alone, the combination instead decreases their improved role on the high-temperature or medium/low-temperature reducibility of CeO_2 catalyst, respectively. But $Ce_{0.95}Zr_{0.05}O_z$-TA still presents stronger H_2-TPR intensity at 500~700 ^oC similar to CeO_2-TA. Finally, the doping of Zr further increases the Brønsted and lewis acid sites of CeO_2-TA by inducing the highly dispersive amorphous sulfate species rather than the highly crystallite $CeOSO_4$ crystal, and $Ce_{0.95}Zr_{0.05}O_z$-TA shows the highest amount of both weak and medium-strong Lewis acid sites, which might be an important reason for its better NH_3-SCR activity.

Experimental

Catalysts preparation

Cerium nitrate ($Ce(NO_3)_3{\cdot}6H_2O$, AR), ammonium bicarbonate (NH_4HCO_3, AR) and hydrogen peroxide (H_2O_2, AR, 30 wt.%) and thiourea ($CS(NH_2)_2$, AR) were used as the precursor, the precipitant, the decomposer and the modified agent to obtain CeO_2 and CeO_2-TA via a one-pot hydrothermal method according to our previous study.[26] In order to investigate the influence of low-quality Zr doping on the NH_3-SCR activity of CeO_2-TA, a series of $Ce_{1-x}Zr_xO_z$-TA (x = 0.025,

0.05, 0.1) catalysts were synthesized by substituting partial $Ce(NO_3)_3 \cdot 6H_2O$ using zirconium nitrate ($Zr(NO_3)_4 \cdot 5H_2O$, AR) where *x* represents the molar ratio of Zr/(Ce+Zr). For comparison, the $Ce_{0.95}Zr_{0.05}O_z$ catalyst was also prepared by keeping the molar ratio of Zr/(Ce+Zr) being 0.05 without adding thiourea as the modified agent. Before the test, the as-prepared catalysts had been calcined at 400 °C in air for 5 h.

Catalyst characterizations and activity test

A range of techniques, including SEM, TEM-EDS, XRD, BET, Raman, XPS, H_2-TPR and Pyridine-IR were used to investigate the influence of Zr doping on the physical-chemical properties of CeO_2 and CeO_2-TA. Details of catalyst characterization are given in the supporting information.

The de-NO_x performance evaluation was performed in a fixed bed micro-reactor using 0.45 g samples (40~60 mesh). The typical reactant gases were composed of 600 ppm NH_3, 600 ppm NO, and 5 vol.% O_2 balanced with 99.999 vol.% N_2 with the corresponding gas hourly space velocity (GHSV) being 200,000 mL/(g · h). A T-350 flue gas analyzer (Testo Company, Germany) was used to monitor the concentrations of O_2 and NO_x in the effluent gas. The NO_x conversions were determined according to the following equations:

$$NO_x \text{ conversion}(\%) = \frac{[NO_x]_{in} - [NO_x]_{out}}{[NO_x]_{in}} \times 100\% \quad (1)$$

Herein, $[NO_x]_{out}$ and $[NO_x]_{in}$ represent the outlet and inlet concentrations of NO_x (NO_x=NO + NO_2) at stable state, respectively.

Declaration of competing interest

The authors declare that they have no known competing financial interests or personal relationships that could have appeared to influence the work reported in this paper.

Acknowledgements

This work was supported by the National Science Foundation of China (NO. 51406118), General program of Shanghai Natural Science Foundation (No. 21ZR1461900), Program of Special Appointment (Eastern Scholar) at Shanghai Institutions of Higher Learning (QD2015017).

Keywords: Selective catalytic reduction (SCR); CeO_2; Thiourea; Zirconium doping; Promotional effect

References

[1] a) Y.K. Yu, C.W. Chen, C. He, J.F. Miao, J.S. Chen, *ChemCatChem* **2019**, *11*, 979-984; b) X. Wu, Y.L. Feng, X.Z. Liu, L.L. Liu, Y.L. Du, Z. Li, *Appl. Surf. Sci*, **2019**, *495*, 143513; c) L. Li, L.B. Duan, Z.H. Yang, Y.M. Wang, W.G. Xiang, *Fuel Process. Technol.* **2021**, *216*, 106742.

[2] a) L. Chen, S. Ren, X.D. Xing, J. Yang, J.L. Li, J. Yang, Q.C. Liu, *J. Environ. Chem. Eng.* **2022**, *10*, 108239; b) Y.H. Zhou, S. Ren, J. Yang, W.Z. Liu, Z.H. Su, Z.C. Chen, M.M. Wang, L. Chen, *J. Environ. Chem. Eng.* **2021**, *9*, 106218; c) X. Wu, R.N. Wang, Y.L. Du, C.L. Zou, H. Meng, X.M. Xie, *Mol. Catal.* **2019**, *467*, 150-160.

[3] H.F. Zhang, Y. Wang, C.Y. Zhai, *Mater. Sci. Semicond. Process.* **2022**, *144*, 106568.

[4] P. Rosha, S.K. Mohapatra, S.K. Mahla, A. Dhir, *Biomass Bioenergy* **2019**, *125*, 70-78.

[5] a) H. Liu, H.J. Chen, S. Wang, J.L. Hu, B. Wang, W.R. Bao, J.C. Wang, L.P. Chan, *J. Environ. Chem. Eng.* **2022**, *10*, 107574; b) H. Yang, L. Jia, J. Haraguchi, Y. Wang, B. Xu, Q.T. Zhang, Z.D. Nan, M. Zhang, T. Ohno, *Catal. Sci. Technol.* **2022**, *12*, 5203-5209; c) J.X. Liu, H.F. Cheng, J.F. Bao, P.F. Zhang, M.M. Liu, Y. Leng, Z.H. Zhang, R.M. Tao, J. Liu, Z. Zhao, S. Dai, *J. Mater. Chem. A* **2019**, *7*, 22977-22985.

[6] a) Y. Gao, T. Luan, W.K. Zhang, H. Li, *Res. Chem. Intermed.* **2019**, *45*, 663-686; b) H.F. Cheng, J.B. Tan, Y.W. Ren, M.J. Zhao, J.X. Liu, H. Wang, J. Liu, Z. Zhao, *Ind. Eng. Chem. Res.* **2019**, *58*, 16472-16478.

[7] Y.X. Lu, L.B. Duan, Z.K. Sun, J. Chen, *Proc. Combust. Inst.* **2021**, *38*, 6513-6520.

[8] W. Tan, C.Y. Wang, S.H. Yu, Y.B. Li, S.H. Xie, F. Gao, L. Dong, F.D. Liu, *J. Hazard. Mater.* **2021**, *416*, 125826.

[9] L.L. Li, P.X. Li, W. Tan, K.L. Ma, W.X. Zou, C.J. Tang, L. Dong, *Chin. J. Catal.* **2020**, *41*, 364-373.

[10] a) B.X. Shen, Y.Y. Wang, F.M. Wang, T. Liu, *Chem. Eng. J.* **2014**, *236*, 171-180; b) L.F. Jia, J.X. Liu, D.Q. Huang, J.C. Zhao, J.N. Zhang, K.X. Li, Z.G. Li, W.S. Zhu, Z. Zhao, J. Liu, *ACS Catal.* **2022**, *12*, 11281-11293.

[11] Y. Jiang, T.Y. Liu, W.Q. Gao, H.W. Ge, Z.D. Yang, R.Y. Lin, X.W. Wang, *Chem. Eng. J.* **2022**, *433*, 134576.

[12] a) X.J. Zhang, T.J. Zhang, Z.X. Song, W. Liu, Y. Xing, *J. Fuel Chem. Technol.* **2021**, *49*, 844-852; b) J.Y. Chen, P. Fu, D.F. Lv, Y. Chen, M.L. Fan, J.L. Wu, A. Meshram, B. Mu, X. Li, Q.B. Xia, *Chem. Eng. J.* **2021**, *407*, 127071; c) J.W. Shi, Y. Wang, R.B. Duan, C. Gao, B.R. Wang, C. He, C.M. Niu, *Catal. Sci. Technol.* **2019**, *9*, 718-730; d) J.F. He, Z.B. Xiong, Y.P. Du, W. Lu, S.L. Tian, *J. Energy Inst.* **2021**, *94*, 85-95.

[13] Z.X. Song, Y. Xing, T.J. Zhang, J.G. Zhao, J.K. Wang, Y.L. Mao, B.L. Zhao, X.J. Zhang, M. Zhao, Z.A. Ma, *Appl. Organomet. Chem.* **2020**, *34*, e5446.

[14] a) H. Hu, K.W. Zha, H.R. Li, L.Y. Shi, D.S. Zhang, Appl. Surf. Sci. 2016, 387, 921-928; b) M. Inada, J. Hojo, *Adv. Powder Technol.* **2022**, *33*, 103647.

[15] T.H. Vuong, J. Radnik, E. Kondratenko, M. Schneider, U. Armbruster, A. Brückner, *Appl. Catal. B* **2016**, *197*, 159-167.

[16] F. Zhao, S.D. Li, Y.F. Chen, *J. Solid State Chem.* **2021**, *300*, 122216.

[17] M. Prasad, K. Ray, A. Sinhamahapatra, S. Sengupta, *J. Mater. Sci.* **2022**, *57*, 2839-2856.

[18] X.J. Yao, J. Cao, L. Chen, K.K. Kang, Y. Chen, M. Tian, F.M. Yang, *Chin. J. Catal.* **2019**, *40*, 733-743.

[19] X.J. Ma, P. Lu, P. Wu, *Ceram. Int.* **2018**, *44*, 15989-15994.

[20] H.Z. Bao, K. Qian, X.Q. Chen, J. Fang, W.X. Huang, *Appl. Surf. Sci.* **2019**, *467-468*, 361-369.

[21] a) X. Sun, R.T. Guo, S.W. Liu, J. Liu, W.G. Pan, X. Shi, H. Qin, Z.Y. Wang, Z.Z. Qiu, X.Y. Liu, *Appl. Surf. Sci.* **2018**, *462*, 187-193; b) N.Z. Yang, R.T. Guo, Y. Tian, W.G. Pan, Q.L. Chen, Q.S. Wang, C.Z. Lu, S.X.

Wang, *Fuel* **2016**, *179*, 305-311; c) W.Y. Yao, X.Q. Wang, Y. Liu, Z.B. Wu, *Appl. Surf. Sci.* **2019**, *467-468*, 439-445; d) J.J. Chen, W.T. Zhao, Q. Wu, J.X. Mi, X.Y. Wang, L. Ma, L.L. Jiang, C. Au, J.H. Li, *Chem. Eng. J.* **2020**, *382*, 122910.

[22] Q.L. Cong, L. Chen, X.X. Wang, H.Y. Ma, J.K. Zhao, S.J. Li, Y. Hou, W. Li, *Chem. Eng. J.* **2020**, *379*, 122302.

[23] a) T. Yi, Y.B. Zhang, J.W. Li, X.G. Yang, *Chin. J. Catal.* **2016**, *37*, 300-307; b) L.X. Chen, V. Agrawal, S.L. Tait, *Catal. Sci. Technol.* **2019**, *9*, 1802-1815.

[24] X.Y. Liu, P.L. Wang, Y.J. Shen, S.Y. Bi, W. Ren, D.S. Zhang, *ACS Catal.* **2022**, *12*, 11306-11317.

[25] a) W. Wang, Z.B. Xiong, J. Jin, W. Lu, H.C. Shi, *J. Environ. Chem. Eng.* **2021**, *9*, 106836; b) L. Zhang, W.X. Zou, K.L. Ma, Y. Cao, Y. Xiong, S.G. Wu, C.J. Tang, F. Gao, L. Dong, *J. Phys. Chem. C* **2015**, *119*, 1155-1163.

[26] W. Wang, Z.B. Xiong, W.F. He, W. Lu, H.C. Shi, *J. Energy Inst.* **2021**, *98*, 322-333.

[27] X. Li, X.S. Li, J.J. Chen, J.H. Li, J.M. Hao, *Catal Commun.* **2016**, *87*, 45-48.

[28] G.L. Chi, B.X. Shen, R.R. Yu, C. He, X. Zhang, *J. Hazard. Mater.* **2017**, *330*, 83-92.

[29] C.X. Li, M.Q. Shen, J.Q. Wang, J. Wang, Y.P. Zhai, *Appl. Catal. A* **2018**, *560*, 153-164.

[30] M. Kong, Q.C. Liu, B.H. Zhu, J. Yang, L. Li, Q. Zhou, S. Ren, *Chem. Eng. J.* **2015**, *264*, 815-823.

[31] T.F. Xu, X.D. Wu, Y.X. Gao, Q.W. Lin, J.F. Hu, D. Wang, *Catal Commun* **2017**, *93*, 33-36.

[32] L.J. Sun, M. Yang, L. Cao, Y. Cao, S.T. Xu, D.L. Zhu, P. Tian, Z.M. Liu, *Microporous Mesoporous Mater.* **2020**, *309*, 110585.

[33] J.Y. Zhou, N. Li, X.R. Wang, L. Xu, H. Zhou, *J. Environ. Chem. Eng.* **2022**, *10*, 108160.

[34] H. Bi, L.X. Zhang, Y. Xing, P. Zhang, J.J. Chen, J. Yin, L.J. Bie, Sens. *Actuators B Chem.* **2021**, *330*, 129374.

[35] A.L. Chibac-Scutaru, V. Podasca, I.A. Dascalu, V. Melinte, *Nanomaterials* **2022**, *12*, 1402.

[36] J. Zhou, K. Wu, W.J. Wang, Y.X. Han, Z.Y. Xu, H.Q. Wan, S.R. Zheng, D.Q. Zhu, *Appl. Catal. B* **2015**, *162*, 85-92.

[37] S.J. Zhao, Y. Wang, L. Wang, Y.L. Jin, *Inorg. Chem. Front.* **2017**, *4*, 994-1002.

[38] a) Q.L. Zhang, Y.P. Zhang, T.X. Zhang, H.M. Wang, Y.P. Ma, J.F. Wang, P. Ning, *Appl. Surf. Sci.* **2020**, *503*, 144190; b) C.X. Li, Z.B. Xiong, J.F. He, X.K. Qu, Z.Z. Li, X. Ning, W. Lu, S.M. Wu, L.Z. Tan, *Appl. Catal. A* **2020**, *602*, 117726.

[39] a) R.Y. Xie, L. Ma, K. Sun, G. Zhou, Z. Qu, N.Q. Yan, *J. Hazard. Mater.* **2021**, *420*, 126545; b) X.Y. Wang, K. Zhang, W.T. Zhao, Y.Y. Zhang, Z.X. Lan, T.H. Zhang, Y.H. Xiao, Y.F. Zhang, H.Z. Chang, L.L. Jiang, *Ind. Eng. Chem. Res.* **2017**, *56*, 14980-14994.

[40] J. Ren, X. Liu, R.H. Gao, W.L. Dai, *J. Energy Chem.* **2017**, *26*, 681-687.

[41] a) W.B. Chen, J.L. Gu, B.N. He, R.D. Duan, L.L. Liu, X.D. Wang, *Ind. Eng. Chem. Res.* **2022**, *61*, 10091-10105; b) Q.L. Zhang, J.H. Zhang, Z.X. Song, P. Ning, H. Li, X. Liu, *J Ind Eng Chem* **2016**, *34*, 165-171.

[42] L. Zhang, L. Zhang, G.C. Xu, C. Zhang, X. Li, Z.P. Sun, D.Z. Jia, *New J. Chem* **2017**, *41*, 13418-13424.

[43] Y.E. Zheng, K.Z. Li, H. Wang, Y.H. Wang, D. Tian, Y.G. Wei, X. Zhu, C.H. Zeng, Y.M. Luo, *J. Catal* **2016**, *344*, 365-377.

[44] a) J.Y. Li, Z.X. Song, P. Ning, Q.L. Zhang, X. Liu, H. Li, Z.Z. Huang, *J. Rare Earths* **2015**, *33*, 726-735; b) B. Liu, C.M. Li, G.Q. Zhang, X.S. Yao, S.S.C. Chuang, Z. Li, *ACS Catal* **2018**, *8*, 10446-10456.

[45] W.X. Zou, C.Y. Ge, M.Y. Lu, S.G. Wu, Y.Z. Wang, J.F. Sun, Y. Pu, C.J. Tang, F. Gao, L. Dong, *RSC Adv.* **2015**, *5*, 98335-98343.

[46] W. Tan, J.M. Wang, L.L. Li, A.N. Liu, G. Song, K. Guo, Y.D. Luo, F.D. Liu, F. Gao, L. Dong, *J. Hazard. Mater.* **2020**, *388*, 121729.

[47] Y. Gao, T. Luan, M.Y. Zhang, W.K. Zhang, W.C. Feng, *Catalysts* **2018**, *8*, 642.

[48] L. Kang, L.P. Han, P.L. Wang, C. Feng, J.P. Zhang, T.T. Yan, J. Deng, L.Y. Shi, D.S. Zhang, *Environ. Sci. Technol.* **2020**, *54*, 14066-14075.

[49] a) X.D. Li, S. Ren, L. Liu, X.D. Xing, L. Chen, J.L. Li, J. Yang, Q.C. Liu, *Fuel* **2023**, *332*, 126103; b) M.A.M. Khan, W.K. Khan, M.N. Khan, A.N. Alhazaa, *J. Mater. Sci. Mater. Electron.* **2019**, *30*, 8291-8300.

[50] Z.Z. Zhou, W.H. Li, Z.M. Liu, *Ind. Eng. Chem. Res.* **2021**, *60*, 15472-15478.

[51] J. Fan, P. Ning, Z.X. Song, X. Liu, L.Y. Wang, J. Wang, H.M. Wang, K.X. Long, Q.L. Zhang, *Chem. Eng. J.* **2018**, *334*, 855-863.

[52] a) H. Hu, X.F. Niu, *J. Mater. Sci. Mater. Electron.* **2018**, *29*, 17178-17186; b) X. Liu, J. Ding, X. Lin, R.H. Gao, Z.H. Li, W.L. Dai, *Appl. Catal. A* **2015**, *503*, 117-123.

[53] a) W.J. Zhang, G.F. Liu, J. Jiang, Y.C. Tan, Q. Wang, C.H. Gong, D.K. Shen, C.F. Wu, *Chemosphere* **2020**, *243*, 125419; b) W. Cai, Q. Zhong, S.L. Zhang, W. Zhao, *Chem. Eng. J.* **2014**, *236*, 223-232.

[54] L. Zhang, L.L. Li, Y. Cao, X.J. Yao, C.Y. Ge, F. Gao, Y. Deng, C.J. Tang, L. Dong, *Appl. Catal. B* **2015**, *165*, 589-598.

[55] a) Z.B. Xiong, Z.Z. Li, C.X. Li, W. Wang, W. Lu, Y.P. Du, S.L. Tian, *Appl. Surf. Sci.* **2021**, *536*, 147719; b) C.X. Li, Z.B. Xiong, Y.P. Du, X. Ning, Z.Z. Li, J.F. He, X.K. Qu, W. Lu, S.M. Wu, L.Z. Tan, *J. Energy Inst.* **2020**, *93*, 1809-1818.

[56] a) P.J. Gong, J.L. Xie, D. Fang, F. He, F.X. Li, K. Qi, *Appl. Surf. Sci.* **2020**, *505*, 144641; b) S.W. Liu, R.T. Guo, X. Sun, J. Liu, W.G. Pan, X. Shi, Z.Y. Wang, X.Y. Liu, H. Qin, *Mol. Catal.* **2019**, *462*, 19-27; c) Z.B. Xiong, W. Wang, J. Li, L.H. Huang, W. Lu, *Mol. Catal.* **2022**, *522*, 112250.

[57] J. Yu, Z.C. Si, L. Chen, X.D. Wu, D. Wang, *Appl. Catal. B* **2015**, *163*, 223-232.

[58] Q. Wu, X.P. Chen, J.X. Mi, S.X. Cai, L. Ma, W.T. Zhao, J.J. Chen, J.H. Li, *ACS Sustain. Chem. Eng.* **2021**, *9*, 967-979.

[59] X.D. Li, Z.T. Han, X.X. Wang, S.L. Yang, G. Liu, Y. Gao, C.L. Li, *J Taiwan Inst Chem Eng* **2022**, *132*, 104144.

[60] Y.K. Zhang, Z.B. Xiong, Q.G. Yang, F. Zhou, W. Lu, H.C. Shi, *J. Environ. Chem. Eng.* **2022**, *10*, 108694.

[61] P. Zhang, P.L. Wang, S. Impeng, T.W. Lan, X.Y. Liu, D.S. Zhang, *Environ. Sci. Technol.* **2022**, *56*, 12553−12562.

[62] M. N. Khan, L.P. Han, P.L. Wang, J.B. He, B. Yang, T.T. Yan, L.Y. Shi, D.S. Zhang, *Chem. Eng. J.* **2020**, *397*, 125535.